Dual modulation of BiOCl: empowering photocatalytic antibiotic degradation through surface Co bond and WS_2 heterojunction

Wenhao Yang[a], Xueling Hu[b], Jing Sun[a], Jiemo Zong[a], Linxing Wang[a], Xiaohang Fang[c,*], Yang Yu[c], Kun Liu[a], Hanbing Zhang[a,*]

[a]*School of Resources, Environment and Materials, Guangxi University, Nanning 530004, PR China.*

[b]*School of Green Building and Low-carbon technology, Guangxi Technological College of Machinery and Electricity, Nanning, 530007, China*

[c]*South China Institute of Environmental Science, Guangzhou 510535, PR China*

**Corresponding author. School of Resources, Environment and Materials, Guangxi University, Nanning, 530004, PR China. Email address: coldicezhang0771@163.com (Hanbing Zhang); South China Institute of Environmental Science, Guangzhou 510535, PR China. Email address: fangxiaohang@scies.org (Xiaohang Fang).*

1. Introduction

1.1 Materials reagents and experimental instrument

Table S1. The chemical reagent, purity, manufacturer and producer of reagents

Chemical reagent	Purity	Manufacturer	Producer
$Bi(NO_3)_3 \cdot 5H_2O$	99.0%	Macklin Biochemical Co., Ltd	Shanghai, China
KCl	99.5%	Guangdong Guanghua Sci−Tech Co., Ltd	Guangdong, Chian
Polyvinyl pyrrolidone K30	GR	Sinopharm Chemical Reagent Co., Ltd	Shanghai, China
Ethylene glycol	99.0%	Guangdong Guanghua Sci−Tech Co., Ltd	Guangdong, China
$Na_2WO_4 \cdot {}_2H_2O$	AR	Sinopharm Chemical Reagent Co., Ltd	Shanghai, China
Thioacetamide	99%	Macklin Biochemical Co., Ltd	Shanghai, China
Oxalic acid	99.5%	Macklin Biochemical Co., Ltd	Shanghai, China
$(CH_3COO)_2Co \cdot {}_4H_2O$	99.5%	Macklin Biochemical Co., Ltd	Shanghai, China
Norfloxacin	98.0%	Macklin Biochemical Co., Ltd	Shanghai, China
$Na_2C_2O_4$	99.0%	Guangdong Guanghua Sci-Tech Co., Ltd	Guangdong, Chian
$Na_2S_2O_3$	99.0%	Guangdong Guanghua Sci-Tech Co., Ltd	Guangdong, Chian
Tert-Butanol	99.0%	Tianjin Damao Chemical Reagent Factor	Tianjin, China
p-Benzoquinone	99.0%	Macklin Biochemical Co., Ltd	Shanghai, China
NaOH	96.0%	Tianjin Damao Chemical Reagent Factor	Tianjin, China
HCl	36.0%-38.0%	Lianjiang Ailian Chemical Reagent Co., Ltd	Guangdong, Chian
Humic acid	99.0%	Shanghai Yuanye Bio-technology Co., Ltd	Shanghai, China
$CaCl_2$	96.0%	Guangdong Guanghua Sci-Tech Co., Ltd	Guangdong, Chian
NaCl	99.0%	Guangdong Guanghua Chemical Factory Co., Ltd	Guangdong, Chian
$MgCl_2$	AR	Shanghai Aladdin Biochemical Technology Co., Ltd	Shanghai, China
$NaCO_3$	99.8%	Guangdong Guanghua Sci−Tech Co., Ltd	Guangdong, Chian
$NaHCO_3$	99.5%	Tianjin Damao Chemical Reagent Factor	Tianjin, China
Na_2SO_4	99.0%	Guangdong Guanghua Sci−Tech Co., Ltd	Guangdong, Chian
Absolute ethanol	99.0%	Guangdong Guanghua Sci-Tech Co., Ltd	Guangdong, Chian
Nafion solution	5.0%	Shanghai Branch, Du Pont China Holding Co., Ltd.	Shanghai, Chian
N,N-Dimethylformamide	99.5%	Macklin Biochemical Co., Ltd	Shanghai, China

1.2 Experimental instrument

Table S2. The instrumentation, model, manufacturer and producer of the main experimental instruments

Instrumentation	Model	Manufacturer	Producer
Water purifier	Medium-RO300	Macklin Biochemical Co., Ltd.	Shanghai, China
Analytical balance	PRACTUM224-1	Sartorius Scientific Instrument Co., Ltd.	Germany
Vacuum drying oven	DZF-600	Xinnuo Instrument Equipment Co., Ltd.	Shanghai, China
Ultrasonic cleaner	KQ3200DA	Kunshan Ultrasonic Instrument Co., Ltd.	Jiangsu, China
High speed centrifuge	H2050R-1	Hunan Xiangyi Centrifuge Co., Ltd.	Hunan, China
Microwave hydrothermal synthesizer	XH-200A	Beijing Xianghu Technology Co., Ltd	Beijing, China
Photochemical reaction instrument	BL-GHX-V	Shanghai Bilon Instrument Co., Ltd.	Shanghai, China
Xenon lamp light source system	CEL-S500/350	China Education Au-light Co., Ltd.	Beijing, China
Electrochemical workstation	CHI760D	Shanghai Chenhua Instrument Co., Ltd.	Shanghai, China
Bruker XRD Goniomerter	A300	Bruker Axs Gmbh Corp.	German
laser Raman spectrometer	InVia Reflex	Renishaw Corp.	England
X-ray photoelectron spectrometer	Thermo Scientific K-Alpha Nexsa	Thermo Fisher Science Corp.	America
Scanning electron microscope	SU 8000	Hitachi High-Tech Corp.	Japan
Transmission electron microscope	G2 F30	Thermo Fisher Science Corp.	America
Ultraviolet spectrophotometer	UV-2500	Shimadzu instrument Corp.	Japan
Ultraviolet-visible near-infrared spectrometer	UV-3600Plus	Shimadzu instrument Corp.	Japan
Ultraviolet photoelectron spectroscopy	Escalab 250XI	Thermo Fisher Science Corp.	America
Vacuum freeze dryer	LGJ-18	Beijing Songyuan Huaxing Technology Development Co., Ltd	Beijing, China
Paramagnetic resonance spectrometer	Bruker A300	Bruker Axs Gmbh Corp.	German
High Performance Liquid Chromatography-Mass Spectrometry	Thermos TSQ Quantum Ultra	Thermo Fisher Science Corp.	America

1.3 Water Parameters

Table S3. The relevant parameters of various actual water bodies

Water bodies	pH	Conductivity ($ms \cdot cm^{-1}$)	Salinity (%)	Sampling point
Ultrapure water	6.6	0.04	0	water purifier (Medium−RO300)
Lake water	7.3	1.41	0	Congzuo Lake, Guangxi University
Tap water	7.8	0.87	0	West campus of Guangxi University
River water	7.7	0.09	0	Xinxu River
Seawater	8.0	48.17	20	Tieshan Port

2. Experimental

2.1 Characterization and Optoelectronic Testing

The crystal structure was determined via X-ray diffraction (XRD, Bruker A24A10) with Cu Kα radiation (λ = 1.54 Å). Micro−morphology and elemental composition of the materials were characterized by scanning electron microscopy (SEM, SU 8000) with an energy dispersive spectroscopy (EDS) and transmission electron microscopic (TEM, JEM-F200). The valence state of surface element was explored by X-ray photoelectron spectroscopy (XPS, K-Alpha) and all the binding energies were calibrated using C 1s peak (284.8 eV). The visible light absorbance property of the samples was observed by UV-visible diffuse reflectance spectrophotometer (UV-vis, UV-3600Plus) at a wavelength scan range of 200–800 nm. The electron spin resonance (ESR) analysis was obtained with a Bruke emxplus (Bruker A300).

Photoelectrochemical measurements, including open-circuit potential-time (OCPT), transient photocurrent response (TPR), electrochemical impedance spectroscopy (EIS), and Mott-Schottky (M-S) analysis, were performed using a CHI-760D electrochemical workstation equipped with a CEL-S500/350 xenon lamp and a standard three-electrode system. The working electrodes were prepared by uniformly dispersing 10 mg of the sample and 5 μL of Nafion solution in 1 mL of absolute ethanol under ultrasonication for 10 min. Then, 50 μL of the resulting suspension was coated onto the conductive surface of an ITO glass substrate (working area: 1 cm^2) and dried at 60 °C for 12 h. A Pt flake (1 cm^2) and a saturated Ag/AgCl electrode served as the counter and reference electrodes, respectively. All measurements were conducted in a 0.5 M Na_2SO_4 electrolyte solution. A 300 W xenon lamp with a 420 nm cut-off filter was used as the visible light source. The transient photocurrent was measured at the OCPT under intermittent irradiation (light on/off cycles: 20 s). EIS spectra were acquired under similar conditions, while the M-S plots were recorded in the dark at frequencies of 500, 800, and 1000 Hz.

The identification of potential degradation intermediates and pathways of norfloxacin (NOR) was

conducted using high-performance liquid chromatography coupled with mass spectrometry (HPLC–MS, Q-EXACTIVE). Water conductivity was determined with an SX823 multiparameter pH/conductivity meter.

2.2 Photocatalysis Experiment

The dark adsorption properties of the synthesized samples were evaluated on the basis of NOR removal. 20 mg of the samples (BiOCl, BiOCl/WS_2, Co-BiOCl, Co-BiOCl/WS_2) were dispersed individually into 50 ml of NOR solution at a concentration of 10 mg·L^{-1}. Subsequently, the suspensions were magnetically stirred continuously for 15 min in a dark environment to achieve sufficient adsorption-desorption equilibrium. During this process, 3 mL of supernatant samples were withdrawn from the catalytic tube at different times and further filtered through a 0.22 μm needle filter. Finally, the concentration changes of the NOR solution was determined by UV-visible spectroscopy.

To evaluate the influence of environmental factors on the photocatalytic degradation process, a series of experiments were conducted under conditions consistent with the standard photocatalytic procedure. The initial pH of the CIP solution was adjusted to approximately 5, 6, 7, 8, and 9 using 0.1 mol·L^{-1} HCl or NaOH, followed by degradation with Co-BiOCl/WS_2 to assess pH-dependent performance. Additionally, the effect of natural organic matter was investigated by introducing humic acid (HA) at concentrations of 1–9 mg·L^{-1} into NOR solutions. The impact of common inorganic ions was examined by adding 2 mM of various cations (K^+, Ca^{2+}, Na^+, Mg^{2+}) and anions (CO_3^{2-}, SO_4^{2-}, HCO_3^-, Cl^-) into the reaction system. Furthermore, the practical applicability of the Co-BiOCl/WS_2 composite was evaluated by performing degradation experiments in different real water matrices spiked with NOR (10 mg·L^{-1}).

The reusability of the Co-BiOCl/WS_2 composite was evaluated over five consecutive photocatalytic cycles. After each run, the spent catalyst was recovered through filtration and centrifugation, thoroughly washed three times with anhydrous ethanol to eliminate surface impurities, and finally collected via freeze-drying. The recycled materials were subsequently reused under identical reaction conditions to assess stability and performance retention. In addition, trapping experiments were performed to identify the primary active species involved in the photocatalytic process. Specifically, sodium oxalate ($Na_2C_2O_4$), sodium thiosulfate ($Na_2S_2O_3$), tert-butanol (TBA), and benzoquinone (BQ) were introduced into the NOR solution at appropriate concentrations to scavenge holes (h^+), electrons (e^-), hydroxyl radicals (·OH), and superoxide radicals ($\cdot O_2^-$), respectively.

3. Results and discussion

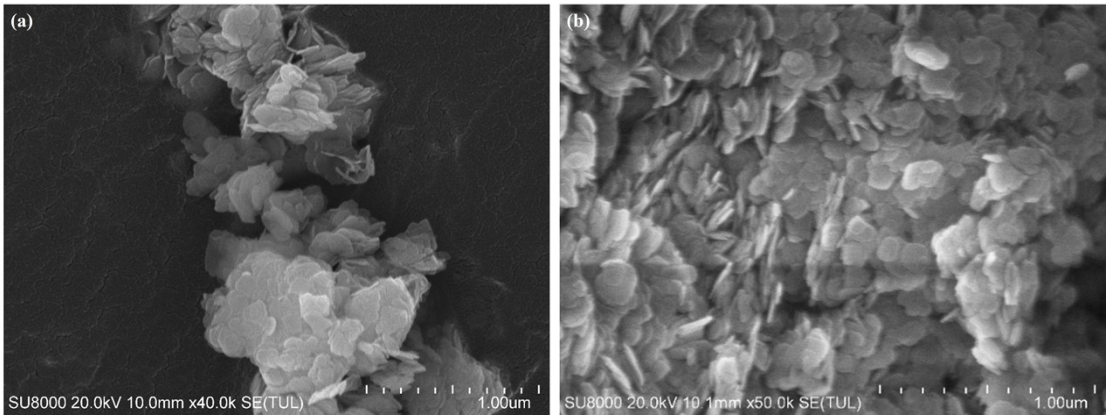

Fig.S1. SEM images of (a) Co-BiOCl, (b) BiOCl/WS_2

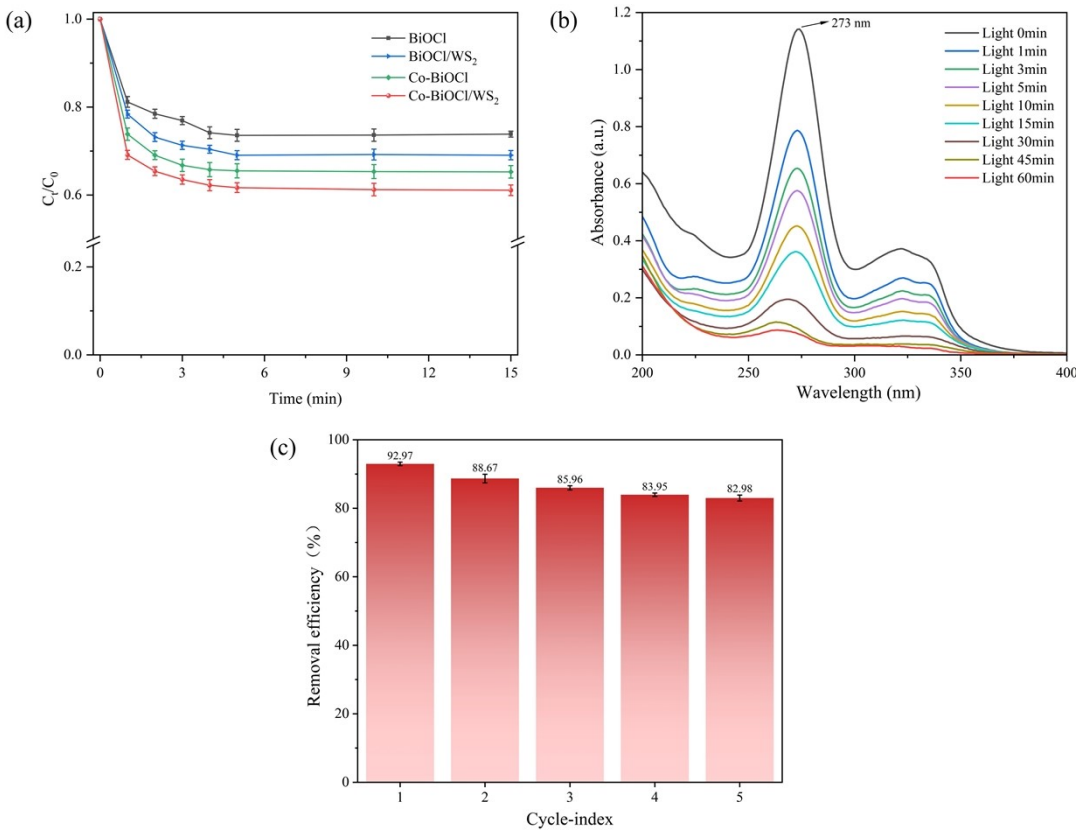

Fig.S2. (a) Dark adsorption experiment of synthetic samples, (b) UV-visible spectrophotometry spectrum of NOR degradation over Co-BiOCl/WS_2, (c) Cyclic Degradation Experiment of Co-BiOCl/WS_2

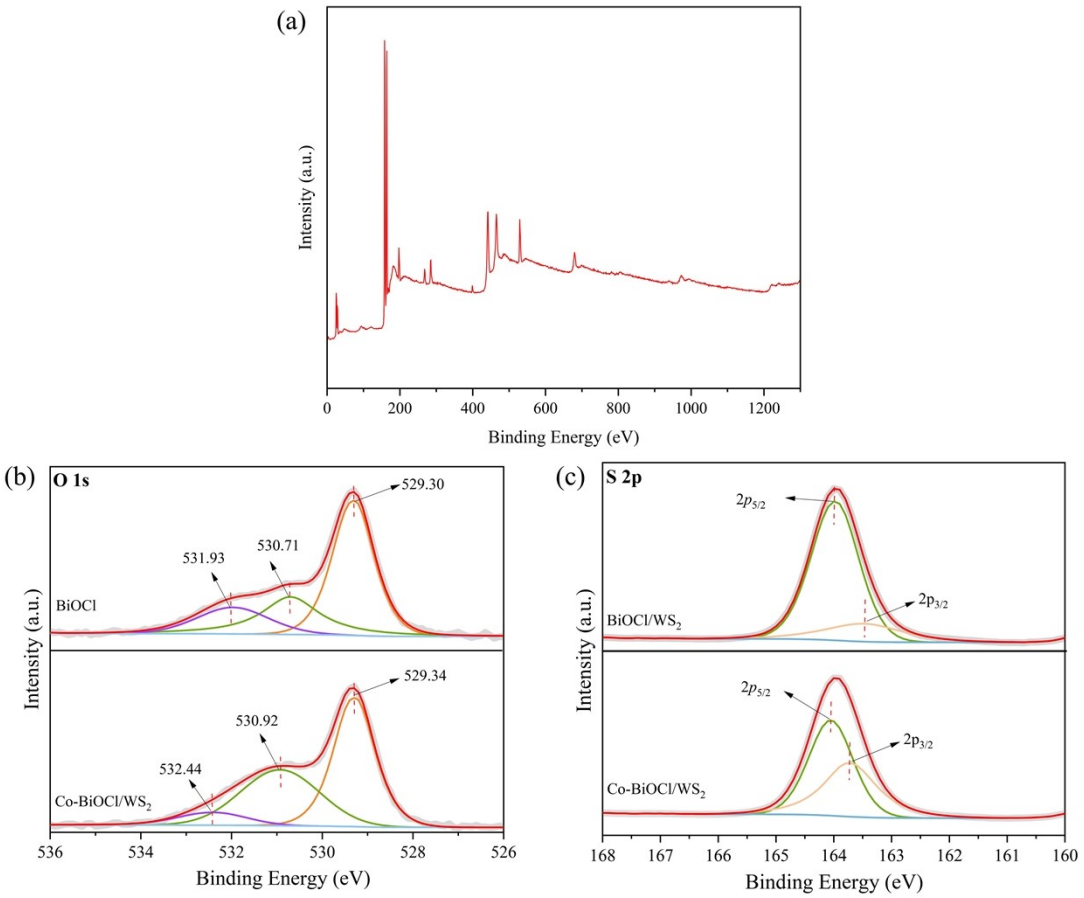

Fig.S3. XPS spectra of (a) full spectra of Co-BiOCl/WS_2, (b) O 1s, (c) S 2p for samples

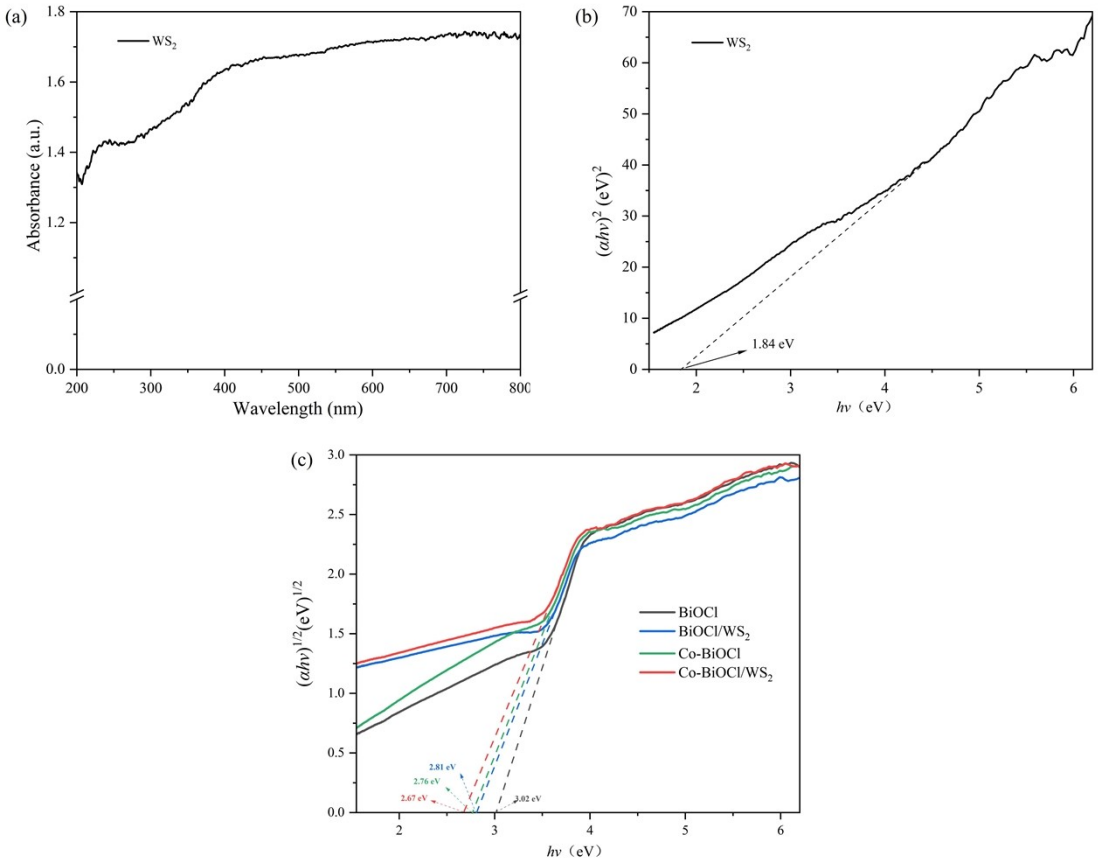

Fig.S4. (a)Uv-vis DRS spectrum of WS_2 and Tauc curve of (b) WS_2, (c) BiOCl, BiOCl/WS_2, Co-BiOCl and Co-BiOCl/WS_2

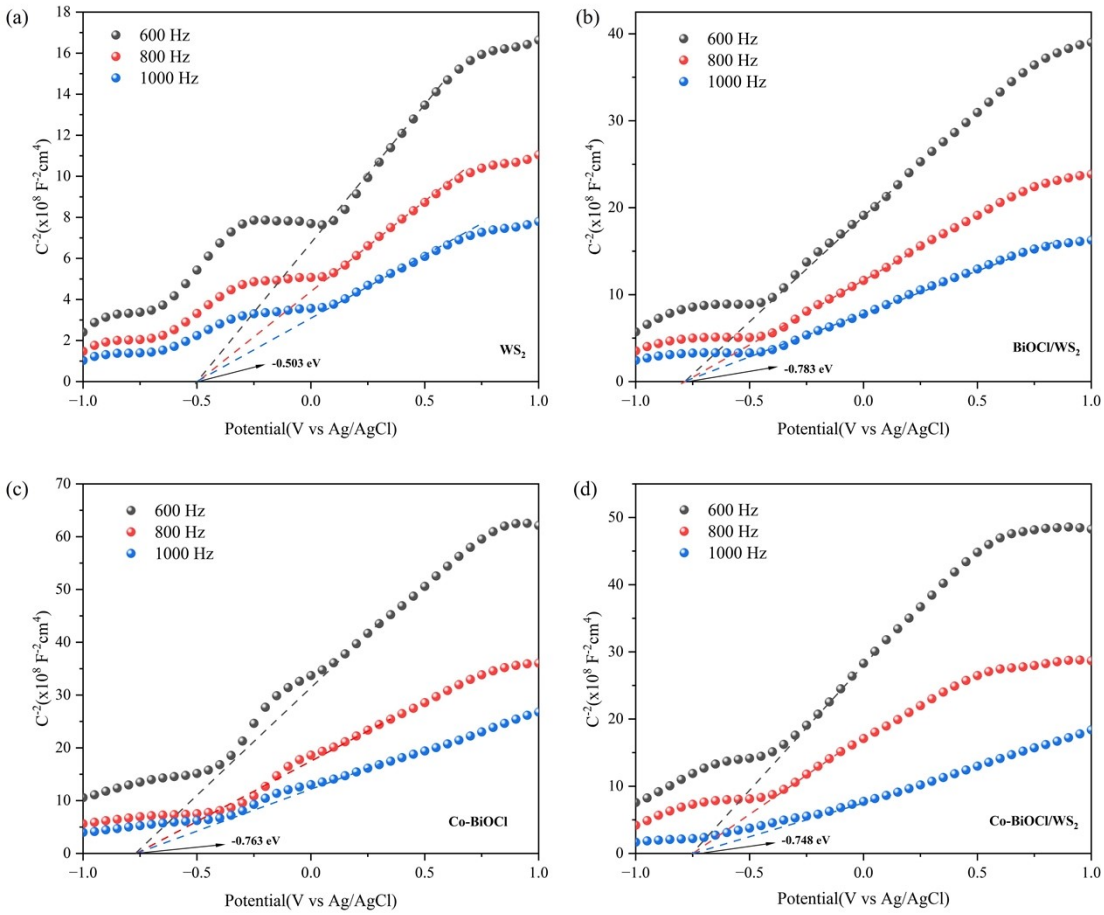

Fig.S5. Mott-Schottky patterns of (a)WS_2, (b)BiOCl/WS_2, (c)Co-BiOCl and (d)Co-BiOCl/WS_2

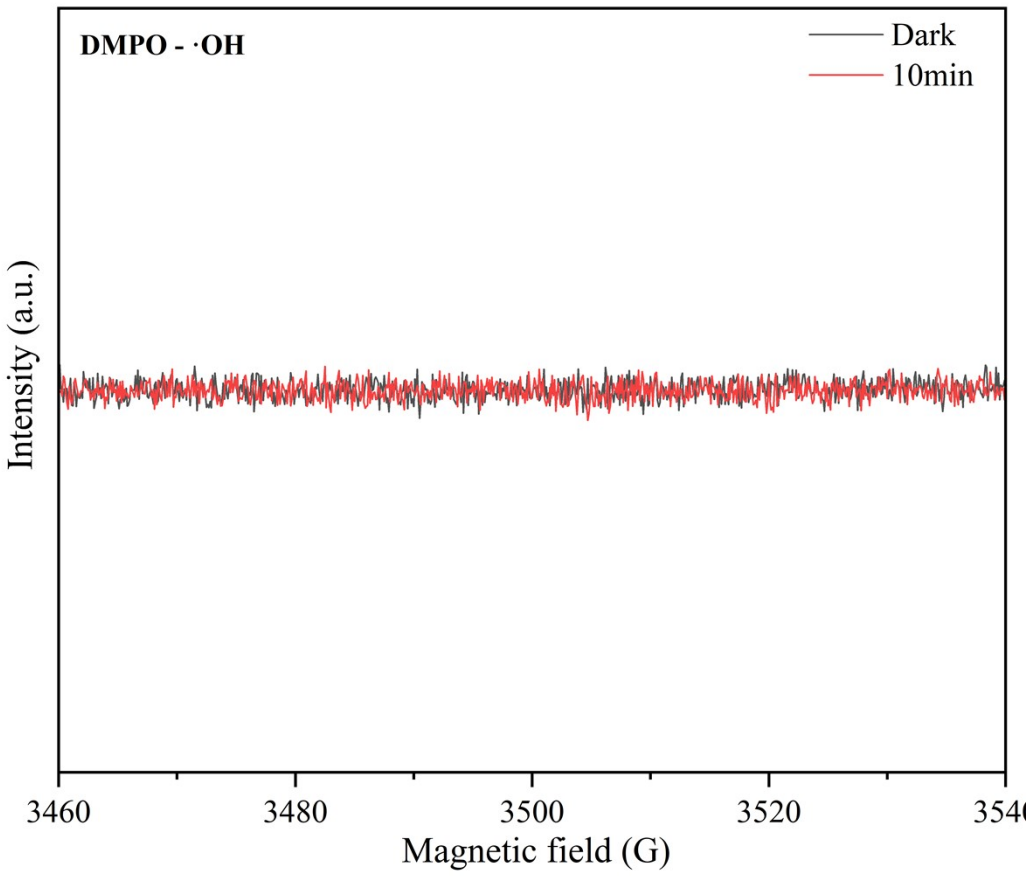

Fig.S6. EPR spectra of DMPO-·OH in Co-BiOCl/WS_2 system under dark and 10 min visible-light irradiation.

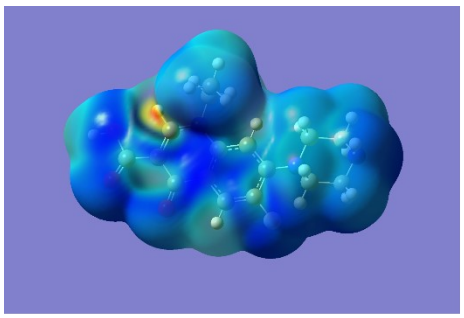

f^+

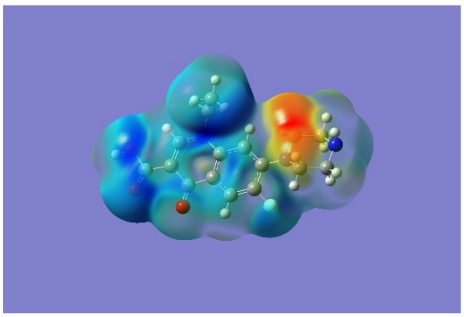

f^-

No.（Atom）	Atom	N	N-1	N+1	F^-	F^+	F^0
1	C	0.08009	0.13024	0.03610	0.05016	0.04399	0.04707
2	C	-0.03837	-0.01298	-0.09692	0.02540	0.05855	0.04197
3	C	-0.03246	0.02225	-0.04041	0.05472	0.00795	0.03133
4	C	0.04084	0.06729	0.02840	0.02645	0.01245	0.01945
5	C	-0.07646	-0.05715	-0.13080	0.01930	0.05434	0.03682
6	C	0.03918	0.06069	-0.00405	0.02151	0.04322	0.03237
7	H	0.05764	0.07842	0.02808	0.02078	0.02956	0.02517
8	C	0.11300	0.13668	0.06468	0.02368	0.04832	0.03600
9	H	0.03293	0.04717	0.00804	0.01424	0.02489	0.01957
10	C	0.03699	0.05708	-0.06828	0.02010	0.10526	0.06268
11	C	-0.05833	-0.02502	-0.09895	0.03332	0.04062	0.03697
12	H	0.05116	0.06847	0.00856	0.01731	0.04259	0.02995
13	F	-0.09019	-0.05195	-0.12322	0.03823	0.03304	0.03563
14	N	-0.06482	0.00779	-0.07785	0.07262	0.01303	0.04282
15	N	-0.15847	-0.10490	-0.17029	0.05357	0.01182	0.03269
16	H	0.09314	0.11551	0.08433	0.02237	0.00881	0.01559
17	C	-0.01400	0.00337	-0.02030	0.01737	0.00630	0.01184
18	H	0.03358	0.04696	0.02944	0.01338	0.00414	0.00876
19	H	0.01528	0.04465	0.00259	0.02937	0.01269	0.02103
20	C	-0.00913	0.00579	-0.01591	0.01491	0.00678	0.01085
21	H	0.03403	0.05016	0.02680	0.01613	0.00723	0.01168
22	H	0.03834	0.06051	0.02494	0.02217	0.01341	0.01779
23	C	-0.01168	0.00530	-0.01607	0.01698	0.00439	0.01069
24	H	0.01461	0.04300	0.00478	0.02839	0.00982	0.01911
25	H	0.03559	0.05098	0.03123	0.01539	0.00436	0.00988
26	C	-0.00914	0.00691	-0.01645	0.01605	0.00731	0.01168
27	H	0.03647	0.05936	0.02292	0.02289	0.01355	0.01822
28	H	0.03311	0.04984	0.02517	0.01673	0.00794	0.01234
29	C	0.01629	0.02359	0.00674	0.00729	0.00955	0.00842
30	H	0.04091	0.04894	0.02359	0.00802	0.01733	0.01267
31	H	0.04670	0.06122	0.02898	0.01453	0.01772	0.01612
32	C	-0.08206	-0.07400	-0.09190	0.00806	0.00983	0.00895
33	H	0.03416	0.03499	0.02667	0.00082	0.00750	0.00416
34	H	0.03999	0.05593	0.01844	0.01594	0.02155	0.01874
35	H	0.03801	0.04781	0.02733	0.00979	0.01068	0.01024
36	N	0.00427	0.03213	-0.02434	0.02786	0.02861	0.02823
37	O	-0.27038	-0.18159	-0.34558	0.08879	0.07520	0.08199
38	C	0.19421	0.20537	0.16641	0.01116	0.02780	0.01948
39	O	-0.26656	-0.23532	-0.31922	0.03123	0.05266	0.04195
40	O	-0.19188	-0.17604	-0.21110	0.01583	0.01922	0.01753
41	H	0.17342	0.19055	0.14744	0.01713	0.02598	0.02156

Fig.S7. Electron clouds f^+, f^- and Hirshfeld charge distributions and condensed Fukui functions for NOR

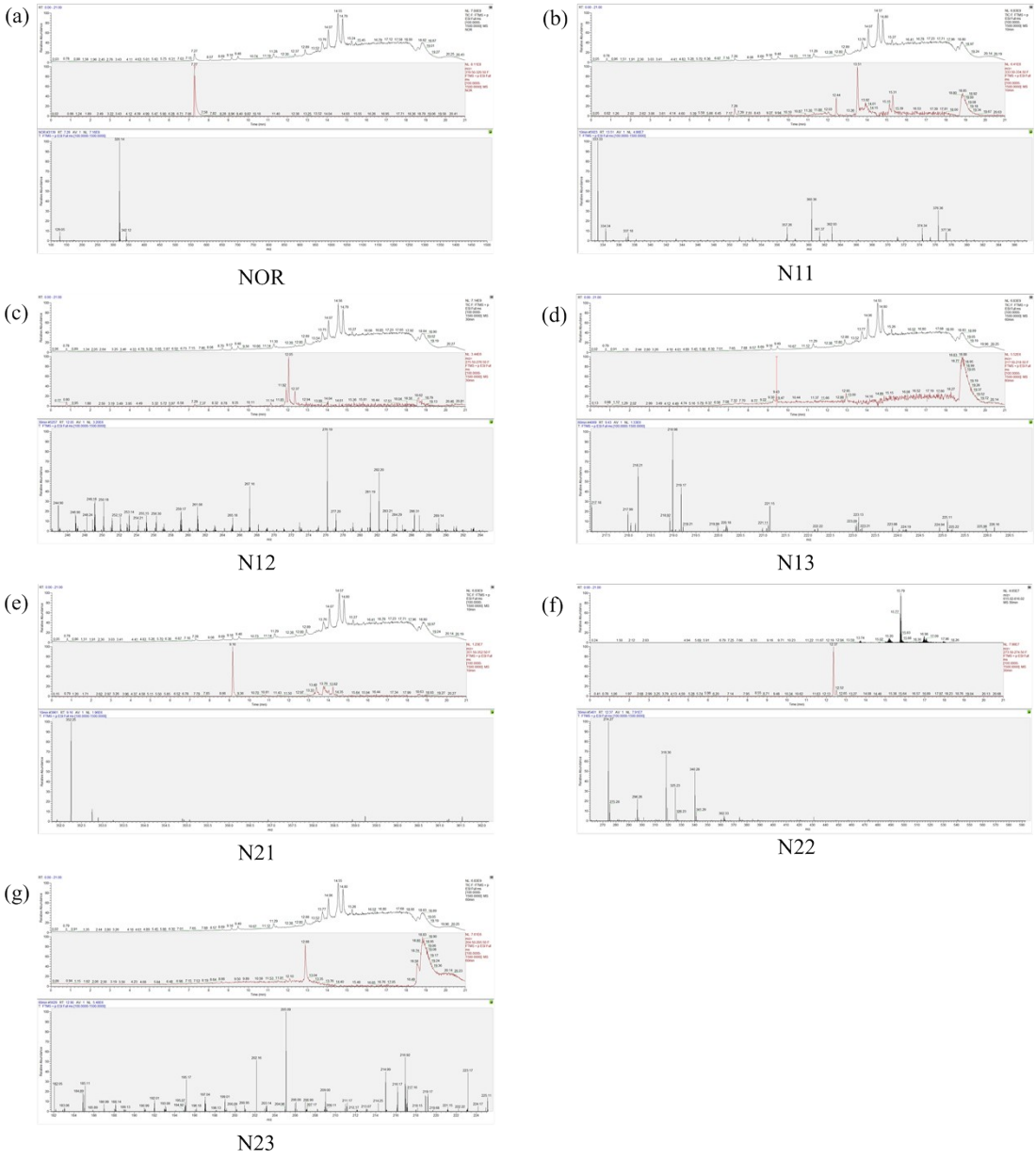

Fig.S8. HPLC-MS spectrum of intermediate products of NOR after photocatalytic degradation over the Co-BiOCl/WS_2. The insets: the corresponding molecular structures and HPLC spectrums.

Table S4. Number, mass-to-charge ratio, and proposed molecular structure of NOR products in degradation pathway.

Product ID	detected mass (m/z)	molecular structure
NOR	320	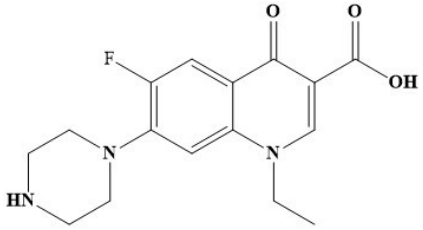
N11	333	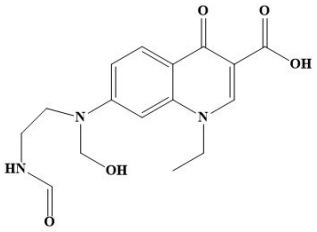
N12	276	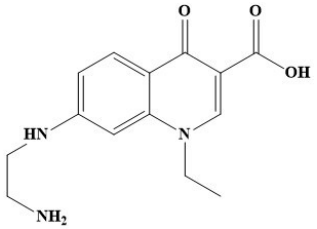
N13	218	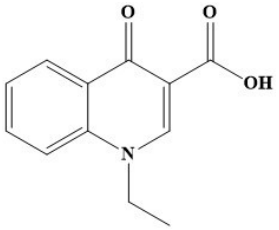
N21	352	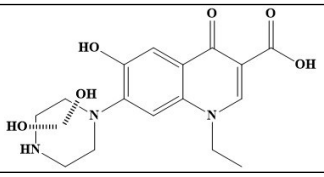
N22	274	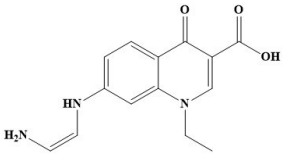
N23	205	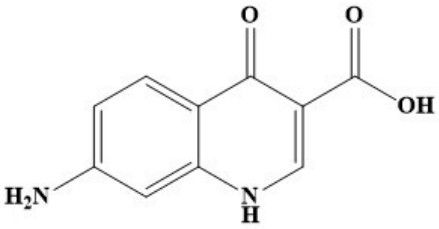

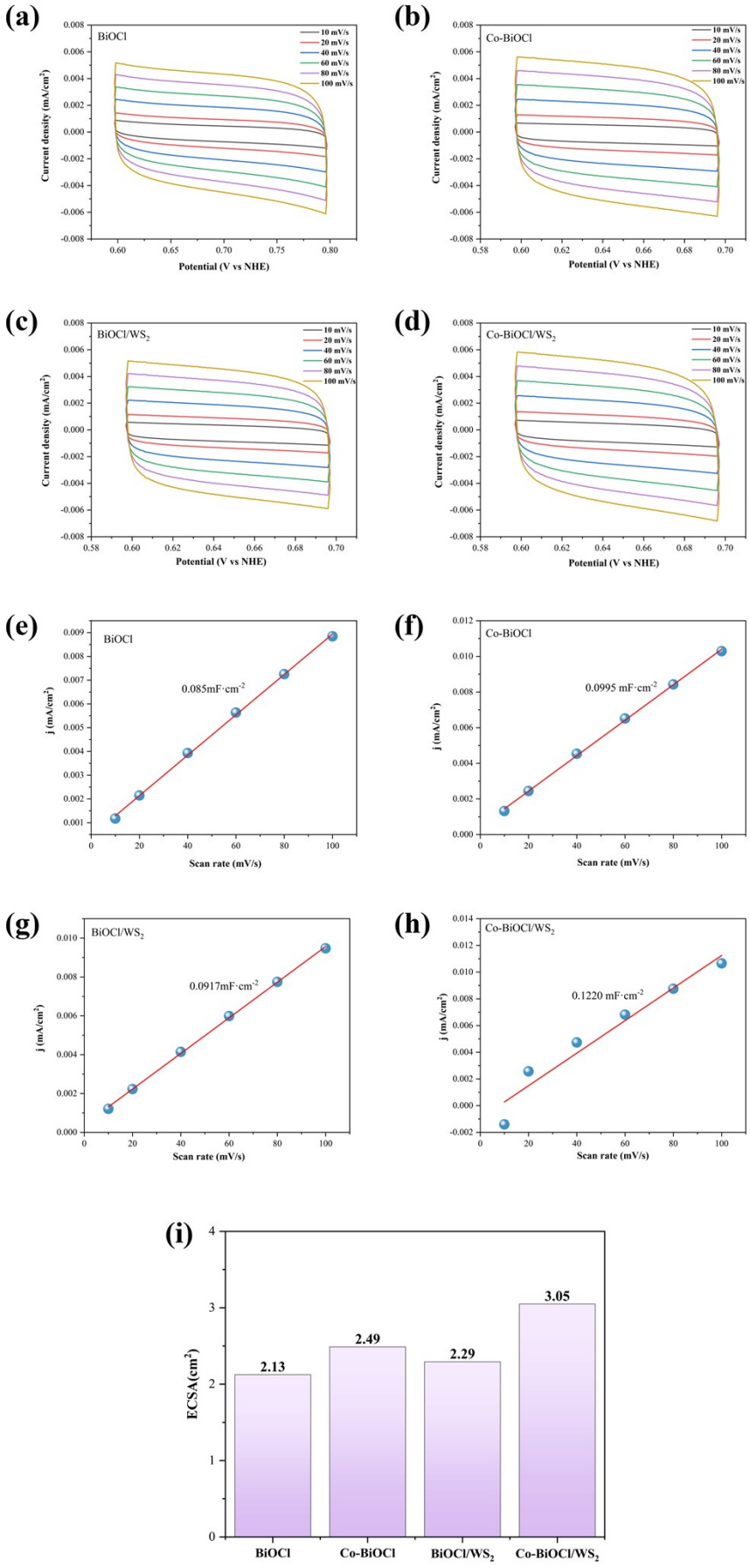
(a)
BiOCl
10 mV/s
20 mV/s
40 mV/s
60 mV/s
80 mV/s
100 mV/s
Current density (mA/cm²)
Potential (V vs NHE)
(b)
Co-BiOCl
(c)
BiOCl/WS2
(d)
Co-BiOCl/WS2
(e)
BiOCl
0.085mF·cm-2
j (mA/cm²)
Scan rate (mV/s)
(f)
Co-BiOCl
0.0995 mF·cm-2
(g)
BiOCl/WS2
0.0917mF·cm-2
(h)
Co-BiOCl/WS2
0.1220 mF·cm-2
(i)
ECSA(cm²)
2.13
2.49
2.29
3.05
BiOCl
Co-BiOCl
BiOCl/WS2
Co-BiOCl/WS2

Fig.S9. Capacitive currents of (a)BiOCl, (b)Co-BiOCl, (c)BiOCl/WS_2 and (d)Co-BiOCl/WS_2; CV curves of (e)BiOCl, (f)Co-BiOCl, (g)BiOCl/WS_2 and (h)Co-BiOCl/WS_2; (i)ECSA of samples

The TOF calculation formula is TOF=I/(α·N·F), in which I is the current density, α is electron number, N is the number of active sites, F is 96485 C/mol. The N could be calculated by density of active sites *ECSA. In the pathway analysis, when NOR is degraded into N13 and N23 products, 22 and 23 electrons are transferred, respectively. For computational convenience, we use a transfer of 20 electrons for comparative calculations (α = 20). Crystal Structure Theory: The surface atomic density of the (001) crystal plane of BiOCl is approximately 1.77×10^{15} atoms/cm^2[1]. Therefore, we assume an activity site density of 1×10^{15} for BiOCl in our calculations.

$$TOF = \frac{I}{\alpha \cdot N \cdot F} \quad \text{(S1)}$$

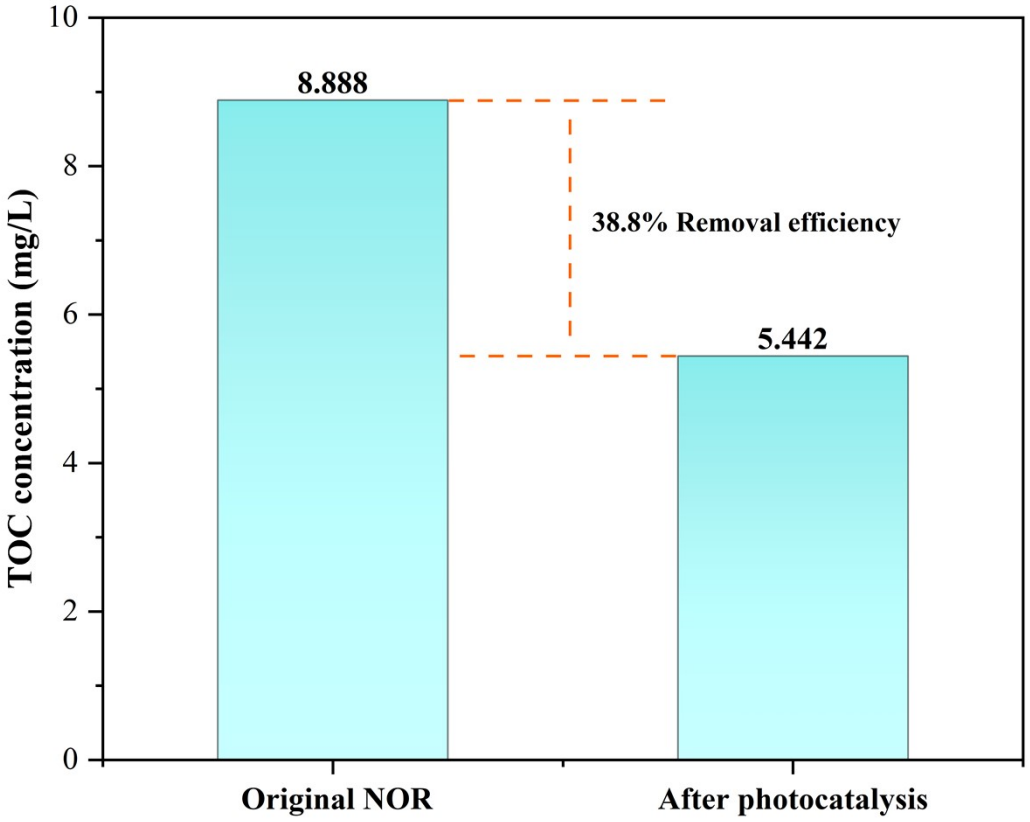

Fig.S10. TOC of NOR before and after photocatalytic degradation by Co-BiOCl/WS_2

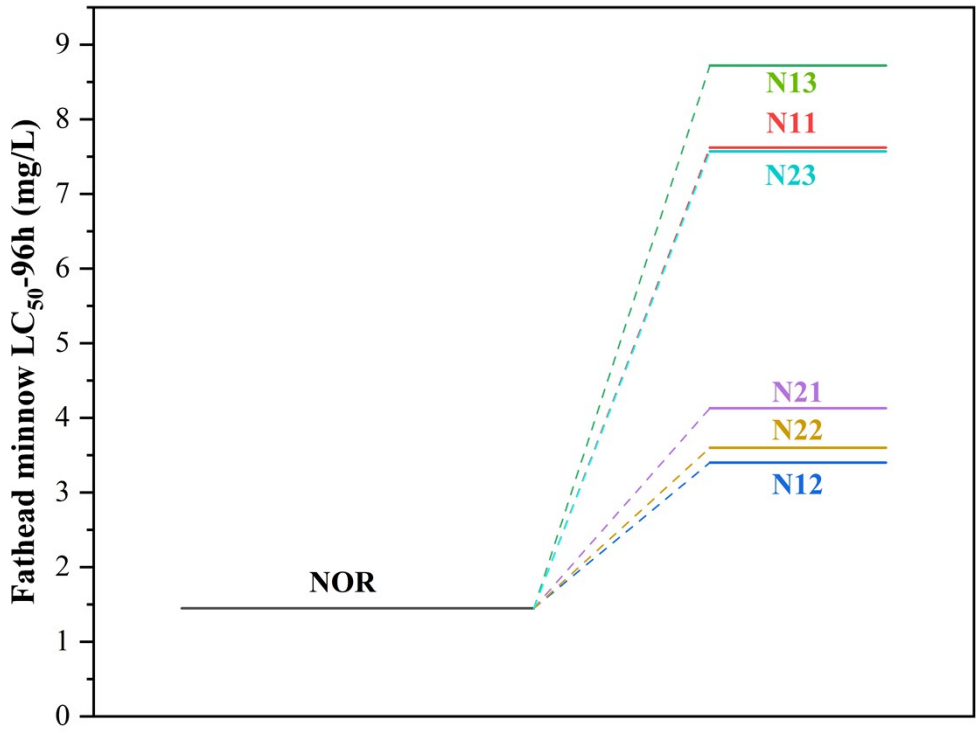

Fig.S11. Acute toxicity LC_{50}-96 h of fathead minnow for NOR and intermediates

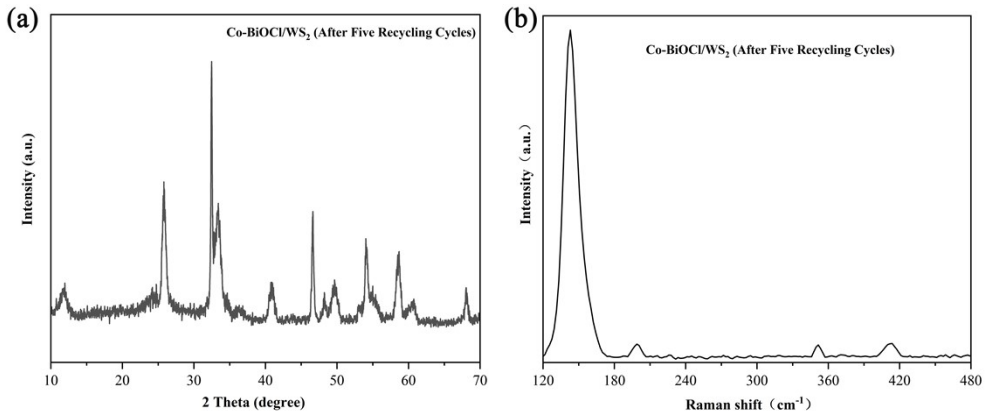

Fig.S12. (a) XRD and (b) Raman of Co-BiOCl/WS_2 after five cycling tests

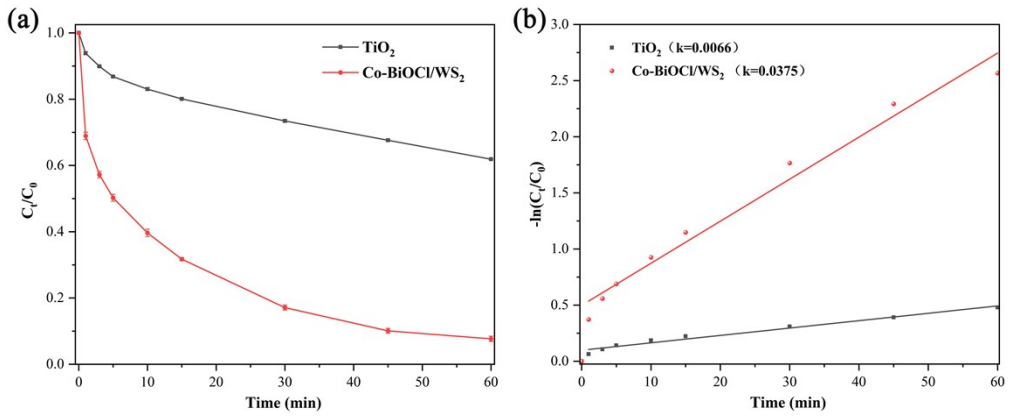

Fig S13. (a) Comparison of photocatalytic degradation of NOR by Co-BiOCl/WS_2 and TiO_2; (b) corresponding pseudo-first-order kinetics

References

[1] G.-Q. Li, X.-C. Zhang, G.-Y. Ding, C.-M. Fan, Z.-H. Liang, P.-D. Han, Study on the atomic and electronic structures of BiOCl{001} surface using first principles, Acta Physica Sinica, 62 (2013) 127301-127301.